Available online at www.sciencedirect.com
ScienceDirect
International Journal of Refractory Metals & Hard Materials 25 (2007) 226–236
International Journal of REFRACTORY METALS & HARD MATERIALS
www.elsevier.com/locate/ijrmhm

Development of niobium powder injection molding. Part II: Debinding and sintering

Gaurav Aggarwal [a], Ivi Smid [a,*], Seong Jin Park [b], Randall M. German [b]

[a] Center for Innovative Sintered Products, The Pennsylvania State University, PA 16802, USA
[b] Center for Advanced Vehicular Systems, Mississippi State University, MS 39762, USA

Received 3 October 2005; accepted 23 May 2006

Abstract

This article is a continuation of feedstock preparation and powder injection molding (PIM) of pure niobium. Part II discusses debinding and sintering of injection molded niobium. PIM of pure niobium powder was analyzed for efficiency of the process. After solvent and thermal debinding, sintering of injection molded material was conducted up to 2000 °C in vacuum as well as inert-gas low-oxygen partial pressure atmosphere. This paper investigates the effect of sintering time, temperature and atmosphere on the processing of pure niobium. Under all sintering conditions the oxygen content is reduced from ~19,000 in the as-received powder to as low as 300 ppm, at e.g. 2000 °C for 2 h in a low-vacuum atmosphere. The carbon content increased from the as-received 70 to 200–300 ppm, depending on the sintering conditions. However, this amount of carbon is not considered detrimental for structural application. Master decomposition and sintering curves are introduced for pure niobium to study the optimum debinding and sintering conditions. Further, sintering parameters (atmosphere, peak temperature and hold time) are optimized for achieving maximum densities with minimal impurities.

Keywords: Nb; Niobium; Powder injection molding; Solvent debinding; Thermal debinding; Sintering of Nb; Master decomposition curve; Master sintering curve

1. Introduction

Niobium is the lightest refractory metal (density = 8.57 g/cc). Approximately 75% of all niobium metal is used as an addition to low-alloyed steels. Another 20–25% is used as an additive in nickel base superalloys and heat-resisting steels. Only 1–2% is used in the form of pure niobium and niobium-base high temperature alloys [1,2]. Due to its limited application and reactive nature during processing, little work has been done in processing of pure niobium. In 1944, for the first time pure niobium powder was pressed into bars and sintered in vacuum by resistance heating [3]. But there were no details on the processing parameters. Since then, reports on the powder metallurgy processing of pure niobium have been erratic. Klopp et al. [4] observed 91% density after sintering niobium bars at 2150 °C for 4 h. The initial powder size was 3.2 μm and final oxygen and carbon contents were 0.079 and 0.03 wt%, respectively. In investigating porous niobium, sintering in the range of 1000–1600 °C under ultra-high vacuum and low-oxygen partial pressure has been done of fairly large powder size (32–63 μm) [5]. In a similar study, fine niobium powder (1.3 μm) was sintered in the range of 1200–1800 °C under vacuum [6]. Both studies provided minimal details with regard to final density and impurity content. Cold isostatically pressed niobium ($D_{50} = 6.7$ μm, $O = 0.62$ wt%) was sintered up to 2000 °C under vacuum [7]. Abnormal grain growth above 1800 °C was observed and the final oxygen content was 0.05 wt%. All of the above work consisted of simple pressing of niobium powder into bars, and little to no work has been done in processing of pure

* Corresponding author. Tel.: +1 814 863 8208; fax: +1 814 863 8211.
E-mail address: smid@psu.edu (I. Smid).

0263-4368/$ - see front matter © 2006 Elsevier Ltd. All rights reserved.
doi:10.1016/j.ijrmhm.2006.05.005

niobium via powder injection molding. Only recently niobium has been introduced as mint metal—via ingot melting and cold deformation [8].

Powder injection molding (PIM) is a relatively new manufacturing process, modified from the plastic injection molding process where a significant volume fraction of the plastic is replaced by small metal particles [1,9]. It is a net-shape process targeted at intricate shapes produced at a high production rate. For refractory metals, PIM as shaping process has a relative cost advantage since it uses the same powders at the same price as used in alternative processes [10]. So, for big lot sizes PIM has a clear economic advantage in producing complex shapes. Dropmann et al. [11], in 1992 applied powder injection molding to Nb-base superalloys. They achieved 94% density after sintering up to 2350 °C.

This article is the second in the series of development of niobium powder injection molding. In Part I [1], the potential of PIM for pure niobium and a systematic approach based on rheological properties were discussed in detail. The primary purpose of Part II is to report the debinding and sintering of injection molded niobium. The discussion covers factors which affect the optimum debinding and sintering conditions. Results are provided for sintered densities, impurity contents (carbon and oxygen), and microhardness. Each of the properties is analyzed against sintering temperature, time, and atmosphere. Finally, an optimum sintering window is provided for niobium based on the master sintering curve (MSC).

2. Experimental procedures

Details on the powder and binder characteristics, feedstock development and injection molding have been detailed in Part I [1], see Table 1. Debinding and sintering of injection molded niobium is described in Part II.

2.1. Solvent and thermal debinding

A two-step debinding process was selected. First, solvent immersion debinding was carried out by immersing the parts in heptane (debinding tank model: 1235; supplier: Sheldon Manufacturing Inc., Cornelius, OR) at 60 ± 1 °C. Parts with a thickness of 3.17 mm were placed on perforated steel trays and dipped into heptane once the temperature reached 60 °C. A debinding time of 2 h was used, which was optimized experimentally using thermo-gravimetric analysis (TGA). Solvent debinding removed most of the wax in the binder, leaving backbone polymers for component handling strength. The next step was to remove the binder by heat. The parts were placed on an alumina setter and debound in a high purity argon atmosphere. After thermal debinding, pre-sintering was done in the same retort to provide handling strength.

2.2. Sintering

Sintering was performed in three different atmospheres at various times and temperatures. The goal was to determine the effect of atmosphere, temperature, and time on the sintered density, impurity content, and mechanical properties. Table 2 shows the set of sintering experiments undertaken. The first three experiments were performed at 1600 °C for three different hold times in atmosphere hV (high vacuum of 1.3×10^{-4} Pa). The next four experiments were performed in higher pressure vacuum (ℓV—low vacuum of 0.13 Pa) at various times and temperatures. The last three runs were performed in a high-purity inert atmosphere (iG—inert-gas low-oxygen partial pressure/argon).

2.3. Property measurement of sintered parts

After sintering, tensile bars were sectioned into two pieces with a diamond cut-off saw and further sectioned on an abrasive cut-off saw. The chips were analyzed for carbon in a combustion carbon/sulfur analyzer (model: EMIA-8200; supplier: JY Horiba, Edison, NJ). A sample weight of 0.5 g was used and three measurements for each sample were performed. Further, the samples were cut to

Table 2
Sintering experiments at various processing parameters

Temperature/time	Atmosphere		
1600 °C/1.0 h	hV	ℓV	–
1600 °C/1.5 h	hV	–	iG
1600 °C/2.0 h	hV	–	–
1800 °C/1.5 h	–	ℓV	–
1800 °C/2.0 h	–	–	iG
2000 °C/0.5 h	–	ℓV	–
2000 °C/1.0 h	–	ℓV	–
2000 °C/1.5 h	–	–	iG

hV—high vacuum.
ℓV—low vacuum.
iG—inert-gas low-oxygen partial pressure.

Table 1
Characteristics of binder components used in binder system [1]

Binder	Paraffin wax	Polypropylene	Polyethylene	Stearic acid
Vendor	Dussek Campbell	PolyVISIONS	DuPont	FisherScientific
Density (g/cm^3)	0.90	0.90	0.92	0.94
Melting range (°C)	42–62	110–150	60–130	74–83
Melting peak (°C)	58	144	122	79
Decomposition range (°C)	180–320	350–470	420–480	263–306

$6.3 \times 6.3 \times 12.6$ mm for oxygen analysis in an oxygen/nitrogen analyzer (model: EMGA-650; supplier: JY Horiba, Edison, NJ). Niobium tends to cover itself with a layer of oxide which cannot be pickled with acid, alkaline, or neutral solutions [12]. So to remove the oxide layer, samples were abraded with a diamond file. After abrading, the samples were cleaned and stored in acetone till testing. Air dried, polished samples with an average weight of 0.5 g were tested for Vickers hardness on a microhardness testing machine (model: M-400-H; supplier: Leco Corporation, St. Joseph, MI). A load of 300 g and a magnification of 40× were selected for the tests. For each sample, five measurements were taken to give an average value and a standard deviation.

3. Theory and model

3.1. Master decomposition curve

The recipe for the powder-binder system of a feedstock often consists of several components. These polymer components may be categorized into two groups according to their molecular weight:

- Low molecular weight polymers, such as solvents and plasticizers, which are either evaporated or are decomposed at low temperatures.
- High molecular weight polymers, such as polymers possessing higher thermal stability which are pyrolyzed at relatively high temperatures.

Therefore, the thermal gravimetric analysis (TGA) curve of such binder systems often has more than two reaction steps. Each reaction step can be described by three kinetic parameters in an Arrhenius-type equation. These parameters are the reaction order n, activation energy Q_D, and frequency factor A. Certain powders have catalytic effects on the rate of pyrolysis. However, the shape of the pyrolysis curve of the binder system with powders is similar to that without powders. Therefore a similar mathematical form of polymer pyrolysis can be applied to feedstocks (mixture of powder and binders).

Typically the TGA curves of degradation of polymers follow a single reaction or sigmoidal path. But some polymers may have two or more sigmoids, where each sigmoid represents a rate-controlling step whose activation energy barrier sufficiently differs from those of the other sigmoids.

Two polymers of the binder system used in this study are decomposed during thermal debinding. The reaction can be of the form

$$\alpha = \omega\alpha_1 + (1-\omega)\alpha_2 \tag{1}$$

where α is the mass ratio of current mass to initial mass of two polymers, α_1 is the mass ratio of low molecular weight polymer, α_2 is the mass ratio of high molecular weight polymer, and ω is the ratio of initial mass of low molecular weight polymer to the initial mass of two polymers.

The mathematical form generally applied to the TGA curve of a polymer is modified to describe the TGA curve of polymer pyrolysis with powders. We assume that the kinetics is solely controlled by temperature.

$$\begin{aligned} -\frac{1}{A\beta^n}\,\mathrm{d}\alpha &= \exp\left[-\frac{Q_D}{R}\left(\frac{1}{T}-\frac{1}{T_t}\right)\right]\mathrm{d}t \\ &\text{if } T \geqslant T_t \text{ (or } \alpha \geqslant \omega), \quad \alpha = \omega\alpha_1 + (1-\omega), \\ &\quad \beta = \frac{\alpha+\omega-1}{\omega}, \quad n = n_1,\ A = A_1,\ Q_D = Q_{D1}, \\ &\text{if } T > T_t \text{ (or } \alpha < \omega), \quad \alpha = (1-\omega)\alpha_2, \\ &\quad \beta = \frac{\alpha}{1-\omega}, \quad n = n_2,\ A = A_2,\ Q_D = Q_{D2} \end{aligned} \tag{2}$$

where R is the universal gas constant, T_t is the transition temperature between the first and second sigmoids, subscripts 1 and 2 on α, n, Q_D, and A denote low-temperature and high-temperature degradation, respectively. A decomposition kinetic curve with more than two sigmoids can also be expressed in a similar manner. The Kissinger method [13] is applied to estimate the activation energy of a reaction.

The left side of Eq. (2) is only a function of the mass ratio α and material properties except for Q_D, which becomes upon integration

$$\Phi_D(\alpha) \equiv \int_1^{\alpha} -\frac{1}{A\beta^n}\,\mathrm{d}\alpha \tag{3}$$

The right side of Eq. (2) is

$$\Theta_D(T) \equiv \int_0^{t} \exp\left[-\frac{Q_D}{R}\left(\frac{1}{T}-\frac{1}{T_t}\right)\right]\mathrm{d}t \tag{4}$$

which depends only on Q_D and the time–temperature profile.

$\Phi_D(\alpha)$ is considered a property of the system that quantifies the effect of binder components on the decomposition kinetics. The relationship between the mass ratio α and $\Phi_D(\alpha)$ is the principle of the master decomposition curve (MDC). Each powder and binder system has a unique MDC which is independent of the decomposition path, given the above assumptions.

3.2. Master sintering curve

For most materials either grain boundary or volume diffusion is the dominant densification mechanism. Surface diffusion is active with small powders, but it does not contribute to densification. The following multiple mechanism model provides a means to predict densification behavior [14]:

$$\frac{\mathrm{d}\rho}{3\rho\,\mathrm{d}t} = \frac{\gamma\Omega}{kT}\left[\frac{\Gamma D_0}{(G)^n}\right]\exp\left(-\frac{Q_\rho}{RT}\right) \tag{5}$$

with $n = 3$ for volume diffusion, and $n = 4$ for grain boundary diffusion. In Eq. (5), γ = surface energy, Ω = atomic volume, k = Boltzmann's constant, Γ = material properties, D_0 = diffusivity preexponent, G = grain size, Q_ρ =

activation energy for diffusion, t = time, and T = absolute temperature. This model assumes grain growth as a function of density. The master sintering curve is a direct consequence of this model [14]. Eq. (5) is rearranged to bring all of the constants and material parameters, and integrated, to create a single density parameter Φ, except for the activation energy as follows:

$$\Phi_\rho(\rho) \equiv \frac{k}{\gamma\Omega} D_0 \int_{\rho_0}^{\rho} \frac{(G)^n}{3\rho\Gamma}\,\mathrm{d}\rho \tag{6}$$

The above integration is from the initial or green density to the target final density. The remaining terms lead to a parameter that is equivalent to the thermal work performed in reaching the density. This parameter Θ_ρ is termed as the work of sintering,

$$\Theta_\rho(t,T) \equiv \int_{t_0}^{t} \frac{1}{T} \exp\left(-\frac{Q_\rho}{RT}\right)\mathrm{d}t \tag{7}$$

Note that the work of sintering Θ_ρ depends on the time-temperature path and contains only the activation energy. While the dominant sintering densification mechanism is volume or grain boundary diffusion, most materials densify through a combination of different densification mechanisms, each changing roles during heating, and as the microstructure changes. For example, grain boundary diffusion is sensitive to the grain size, so grain growth changes its contribution as the grain boundary area declines. Because of these mixed events and their complex dependence on temperature, grain size, surface area, and curvature, the apparent activation energy used in Eq. (7) often does not match a handbook diffusion parameter. Instead, the apparent activation energy is better found using error analysis. The data is lumped into a single set irrespective of heating rates. A function is fitted to the data, the predicted and the residual are computed at each data point. Then the mean square residual is computed. The mean square residual is plotted as a function of activation energy, and the activation energy of the minimum mean residual is chosen as the activation energy for the sintering process. The master sintering curve (MSC) can be generated from measured densities as a function of Θ_ρ, using isothermal or non-isothermal methods as long as the temperature is known, and is a function of time during the sintering cycle.

4. Results and discussion

4.1. Solvent and thermal debinding

As mentioned earlier, a two-step debinding process was used to debind injection molded niobium. Samples tended to crack during thermal debinding when they were not solvent debound. This happens because of the narrow melting range of the filler phase (wax) of the binder system. Thermal debinding was performed in a high-purity argon atmosphere, as niobium reacts with nitrogen or air to form niobium nitride which is brittle and also leads to distortion of the parts. Fig. 1 shows tensile bars under various debinding conditions and final sintered parts.

Fig. 2 gives the thermo-gravimetric analysis (TGA) of the binder system used at three different heating rates.

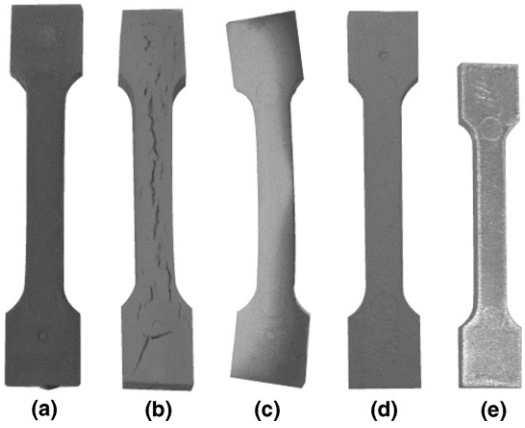

Fig. 1. Powder injection molded Nb bars: (a) green; (b) after thermal debinding without solvent debinding; (c) after solvent debinding followed by thermal debinding in nitrogen; (d) after solvent debinding followed by thermal debinding in argon; (e) sintered.

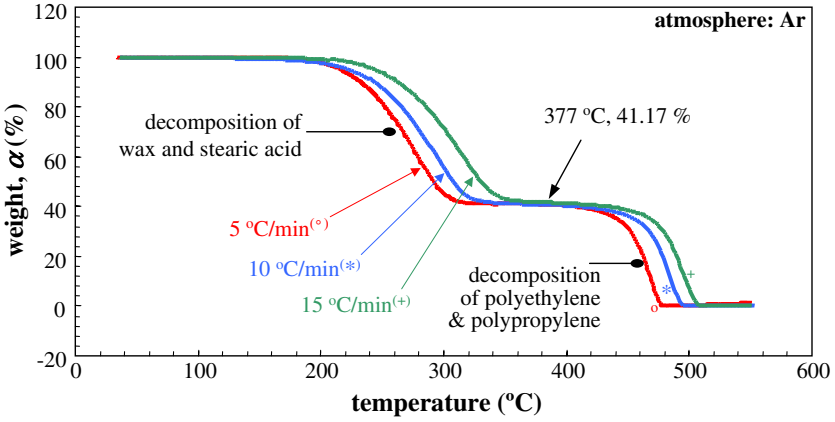

Fig. 2. Thermo-gravimetric analysis (TGA) of the binder system at three different heating rates.

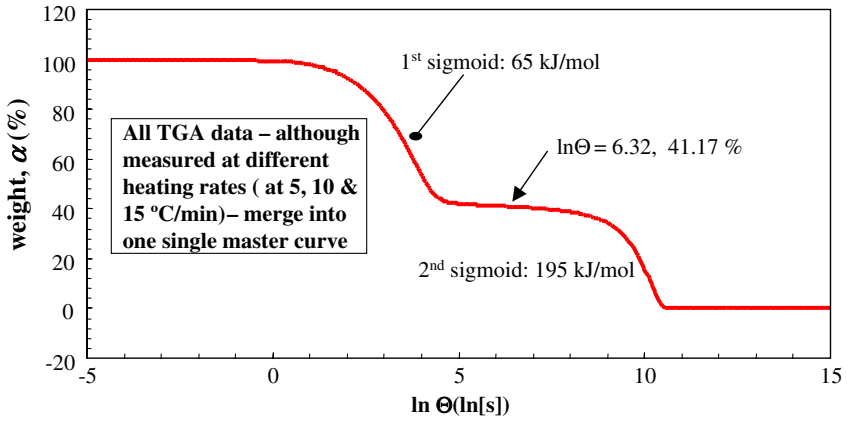

Fig. 3. Master decomposition curve of Nb feedstock 57 vol% solids loading (binder composition see [1]).

The TGA curve at each heating rate has two reaction steps, which gives the amount of binder left during the debinding process. The master decomposition curve (MDC) of this binder system is plotted in Fig. 3. The predicted MDC is in good agreement with the experiments.

4.2. Sintering (hV = high vacuum; ℓV = low vacuum; iG = inert-gas low-oxygen partial pressure)

Three processing parameters (temperature, time and atmosphere) were considered to describe the sintering behavior of the injection molded niobium. Fig. 4 shows the effect of each parameter on the sintered density. Density in high vacuum atmosphere hV increases with hold time, but it is still low in comparison to atmospheres iG and ℓV. Sintering at 1600 °C in atmosphere hV led to poorly dense material, with a substantial amount of porosity. Fig. 5 shows the optical micrograph of niobium sintered at 1600 °C for 1.5 h in hV. It can be clearly seen that the sample has low density (~40% porosity). The grain size remains almost the same as in the starting powder (~7 μm). This is due to a lack of surface diffusion and almost negligible bulk transport at this temperature and time. It was surprising that the sintered density was higher in a low vacuum ℓV with the same peak temperature and hold time as in a high vacuum hV. By increasing the hold time to 2 h, the sintered density increased to 85%; but this led to grain growth, which resulted in deterioration of material properties. The density achieved in atmosphere iG is lower than in ℓV at this temperature, in spite of a longer hold time in atmosphere iG. This happens because the vacuum enhances the elimination of pores, and such promotes densification. Therefore a higher density is achieved in vacuum for niobium as compared to an inert-gas low-oxygen partial pressure (iG) atmosphere. It can be concluded that at 1600 °C, the maximum density (~87%) in niobium can be achieved in a graphite vacuum furnace. But this density is significantly lower than the theoretical density; so to improve the density either the sintering temperature or the hold time should be raised. Klopp et al. [4] concluded that the sintering temperature affects oxygen removal more than the hold time. Taking this into consideration, the next set of experiments were done in iG and ℓV atmospheres at 1800 and 2000 °C with similar hold times as at 1600 °C. The densities achieved in atmosphere ℓV were higher at both 1800 and 2000 °C with a shorter hold time as compared to atmosphere iG due to aforementioned reasons.

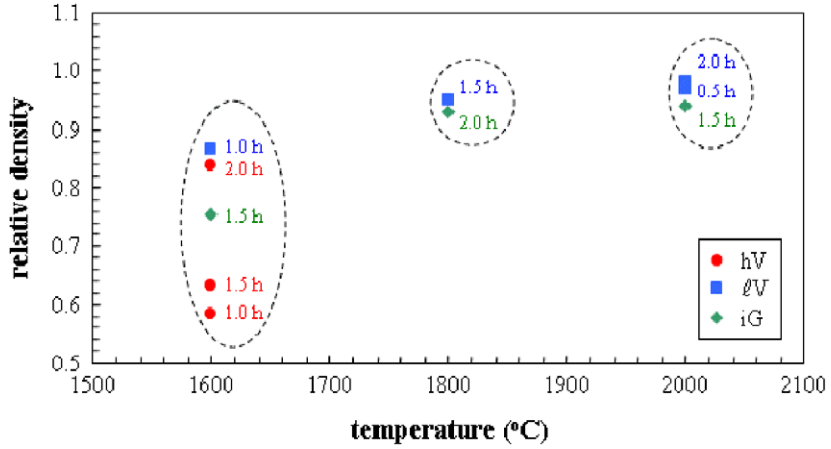

Fig. 4. Effect of processing parameters on sintered density.

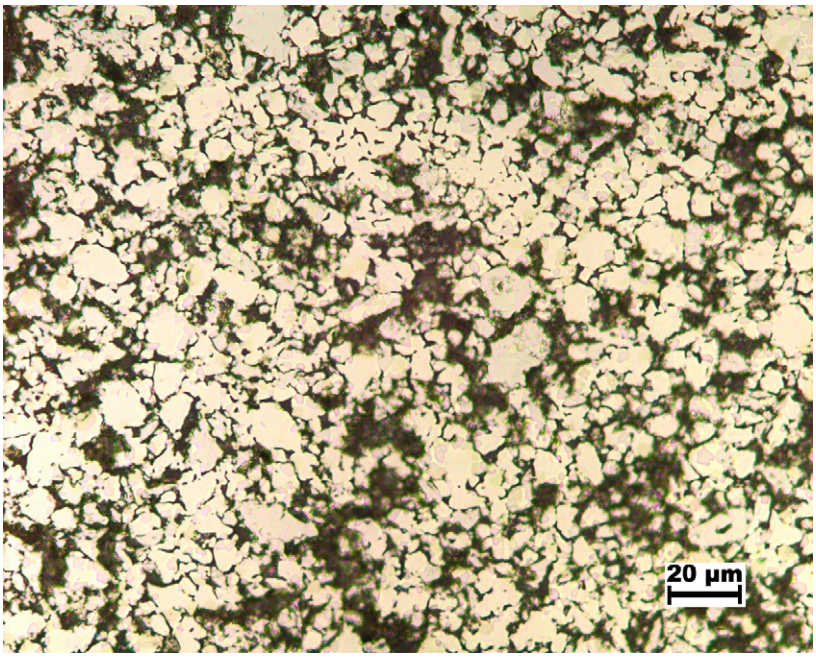

Fig. 5. Micrograph of niobium sintered at 1600 °C/1.5 h in atmosphere hV.

At temperatures above 1800 °C, densification occurs mainly due to bulk transport (volume and surface diffusion) mechanisms, as these mechanisms are more active at high temperatures [15]. The mobility of the grain boundaries also increases at these temperatures and leads to boundary breakaway resulting in formation of newer and bigger grains and pore trapping inside these grains.

Oxygen also plays an important role in the processing of niobium. The oxygen diffuses into the niobium particles, which results in formation of solidified NbO_2 (melting point 1915 °C), NbO, and an O-containing solid solution according to the Nb–O phase diagram (Fig. 6a [17]). The liquid serves to build up inter-particle necks very fast by an enhancement of the material transport into the neck region. It can be seen in Figs. 7 and 8 that excessive grain growth occurs after sintering niobium at 2000 °C. When abnormal grain growth takes place, the few grains that are distributed elsewhere become much larger than the average grain size. Changes in the texture tend to become more pronounced when abnormal grain growth occurs [16].

The X-ray diffraction done on the polished samples shows only niobium (Fig. 9).

Fig. 10 gives the master sintering curve (MSC) for niobium. It can be used to predict densification at various sintering temperatures and hold times in different atmospheres. An activation energy of 263 kJ/mol for grain boundary diffusion during sintering has been used.

4.3. Chemical analysis

The specification limits of carbon and oxygen for good commercial quality niobium components are 0.01 and 0.02 wt%, respectively. The carbon content has to be kept low (below 0.072 wt%) to avoid embrittlement caused by niobium carbide. In this work, concern for carbon control was even higher because of the addition of binders during injection molding. Binders are normally hydrocarbon chains and act as the source for carbon. Rather than going into solid solution, niobium forms niobium carbide already at a fairly low carbon content, which is stable up to 3600 °C, as seen in the phase diagram of Nb–C (Fig. 6b [17]). An increase in carbon content was observed in the final sintered sample from the as-received powder (Table 3). The combination of solvent and thermal debinding gives lower carbon contents as compared to only thermal debinding. This is due to dissolution of wax during solvent debinding, leaving an open pore structure for subsequent binder burnout.

The amount of oxygen in the as-received powder was fairly high (1.9 wt%). The values of oxygen content in sintered samples are plotted vs. sintering temperature (Fig. 11). The oxygen content decreases with increasing sintering temperature for all investigated atmospheres. The lowest oxygen amount is observed after sintering at 2000 °C for 2 h in ℓV. It was also observed that oxygen removal is more affected by the sintering temperature than by hold time. The same dependence of sintering temperature and hold time on oxygen removal was observed in both, ℓV and iG. This can be explained on the basis of the niobium oxygen phase diagram (Fig. 6a). In literature, it has been reported that the removal of oxygen is mainly based on the evaporation of the niobium oxides, which are volatile in nature [18]. Atomic oxygen can also get desorbed at very high temperatures and high oxygen concentrations. Above 1800 °C, the oxygen absorption is

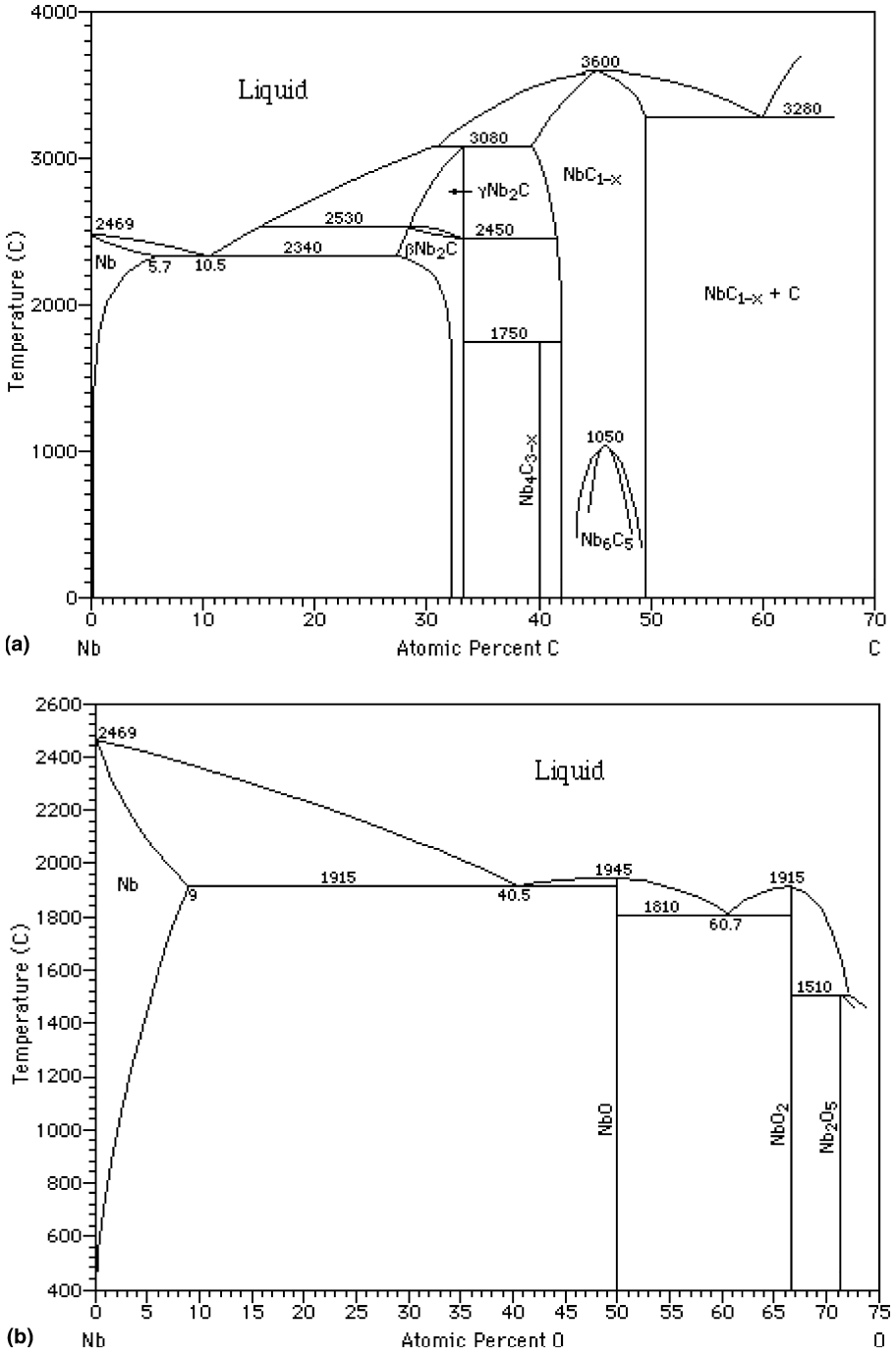

Fig. 6. (a) Nb–O phase diagram; (b) Nb–C phase diagram.

proportional to the pressure [19], therefore, a lower oxygen content is observed under ℓV as compared to iG atmosphere.

The removal of carbon not only depends on the sintering temperature and time, but also on the oxygen content. The first reaction to occur as the molded samples are heated is the reaction between oxygen and carbon to form carbon monoxide (CO). The reaction rate at a given temperature depends on the concentrations of oxygen and carbon in the solid material, diffusivities of oxygen and carbon, the equilibrium pressure of the reaction product, and the ambient pressure. The equilibrium vapor pressure of CO over niobium containing carbon and oxygen at any given temperature decreases as carbon and oxygen contents decrease. The rate of CO evaporation would be expected to decrease. However, as long as the ambient pressure is lower than the equilibrium pressure, carbon and oxygen will continue to diffuse to the surface and evaporate as CO. As the impurities are reduced to low concentrations, and provided that the ambient pressure is lower

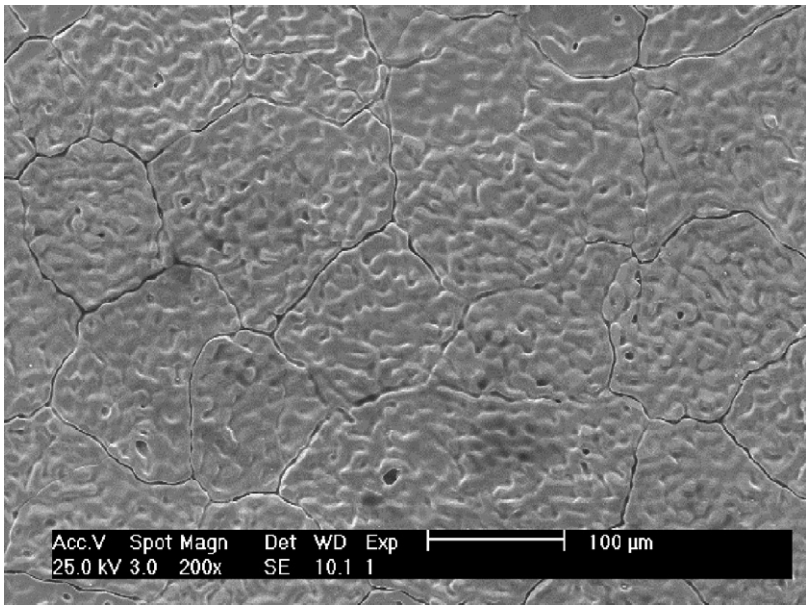

Fig. 7. Micrograph of niobium sintered at 2000 °C/0.5 h in atmosphere ℓV.

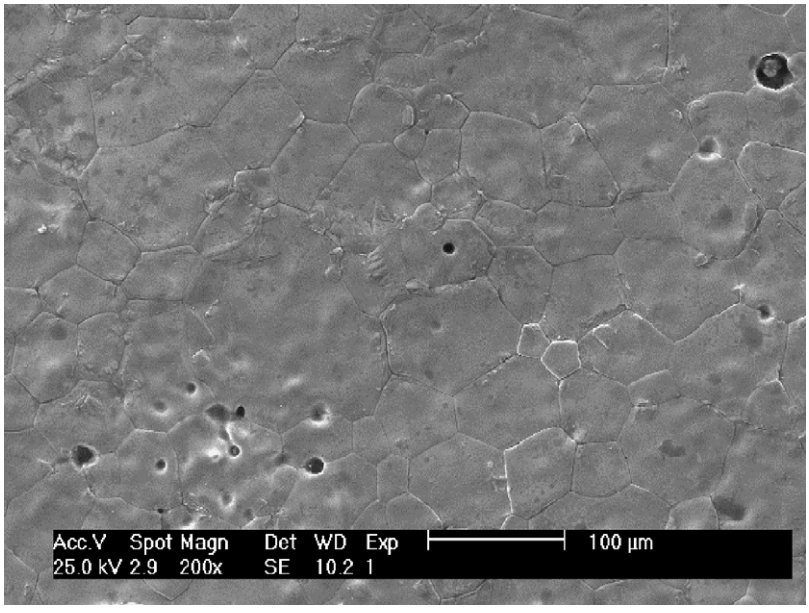

Fig. 8. Micrograph of niobium sintered at 2000 °C/1.5 h in atmosphere iG.

than the equilibrium CO pressure corresponding to the surface concentrations of carbon and oxygen, diffusion of carbon or oxygen to the surface becomes the rate determining step for the entire reaction during sintering.

4.4. Mechanical properties

It was attempted to correlate the hardness with the oxygen and carbon contents after sintering. The oxygen content was related to hardness, but no simple dependence between hardness and carbon content was observed. Fig. 12 gives the relation between microhardness of sintered samples versus the impurity (carbon and oxygen) contents. The hardness tends to increase with increasing oxygen content in the sintered samples. The relationship between microhardness and carbon content is atmosphere dependent. After consolidation in vacuum a higher hardness is observed in samples with lower carbon contents in contrast to samples sintered in an inert-gas low-oxygen partial pressure (iG) atmosphere.

Grain growth, which occurs with the increase in sintering temperature and hold time, results in lowering the grain boundary area. The lesser the grain boundary area the longer the dislocation slip without impediments (low work

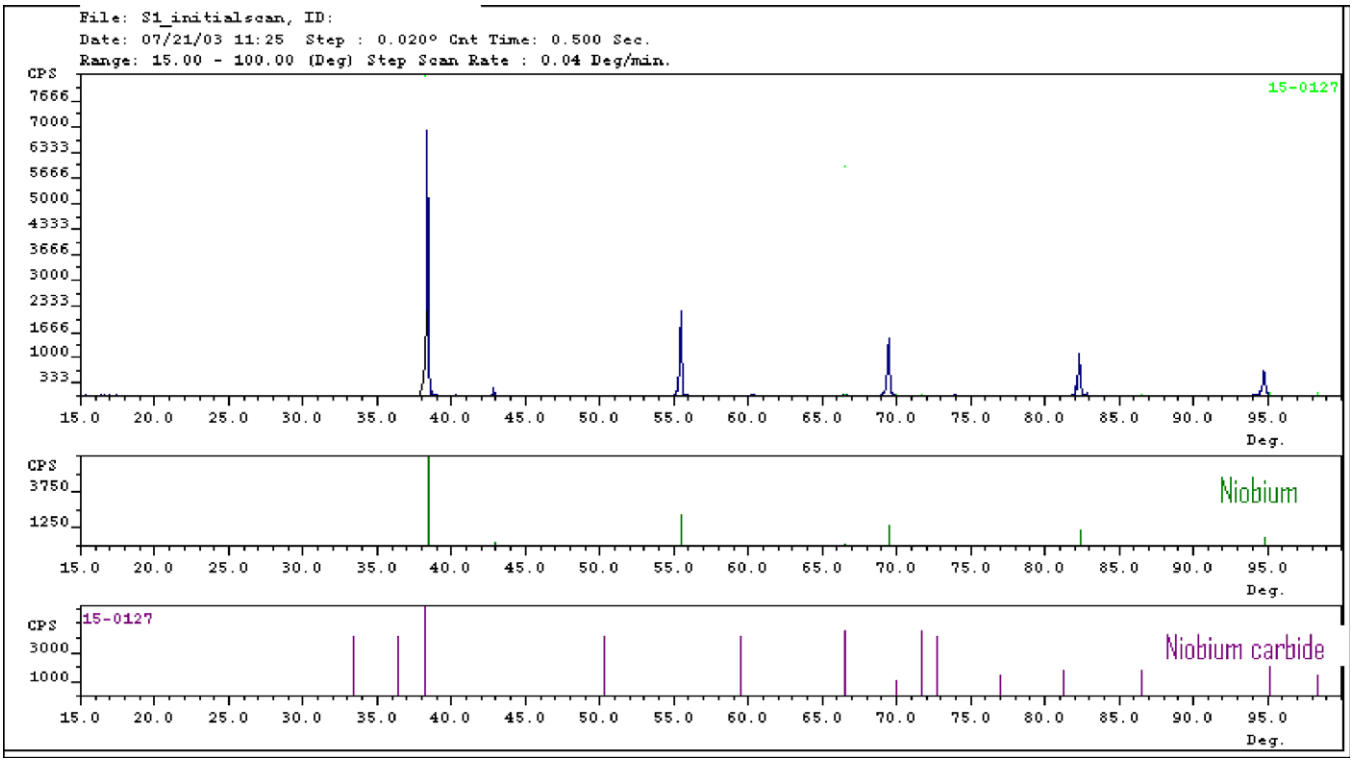

Fig. 9. X-ray diffraction of niobium sintered at 2000 °C/0.5 h in atmosphere ℓV; no niobium carbide is visible.

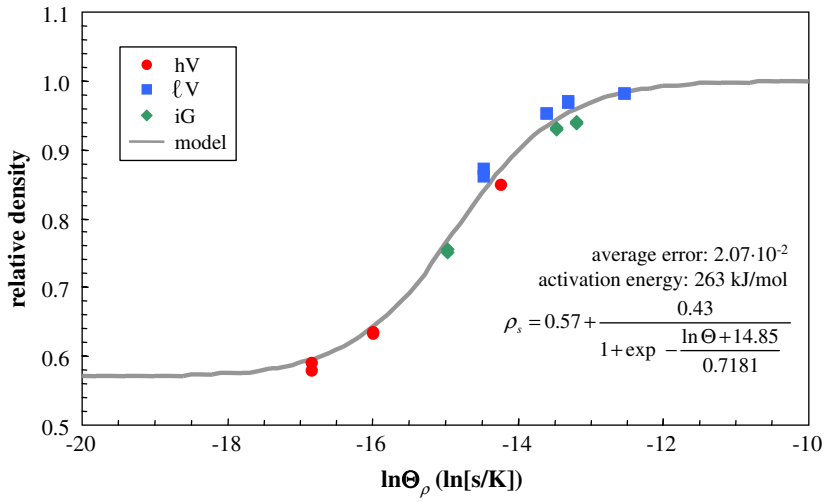

Fig. 10. Master sintering curve for 7 μm powder-injection-molded Nb.

Table 3
Carbon and oxygen content (ppm) during PIM processing of niobium, and sintering at 2000 °C

	As-received	After dehydration	After thermal debinding	After solvent and thermal debinding	After sintering
Carbon	70	30	3820	2270	200[a]
Oxygen	18,977	7800	12,724	1280	300[b]

[a] Sintering at 2000 °C/0.5 h in atmosphere ℓV.
[b] Sintering at 2000 °C/2.0 h in atmosphere ℓV.

hardening), thereby decreasing the resistance to indentation. Grain growth has been observed in the sintered samples as a consequence of both, increase in hold time and sintering temperature. However, even the hardness of samples sintered in the graphite vacuum ℓV furnace decreased with an increase in hold time and sintering temperature.

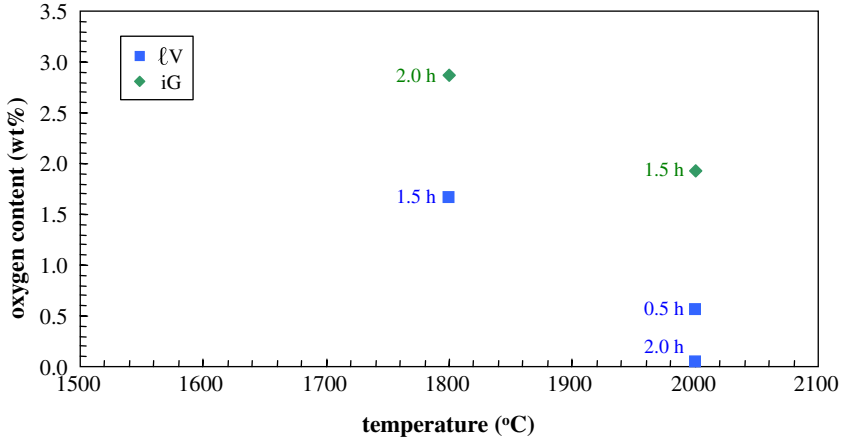

Fig. 11. Oxygen content vs. sintering temperature (1800 or 2000 °C) in various atmospheres.

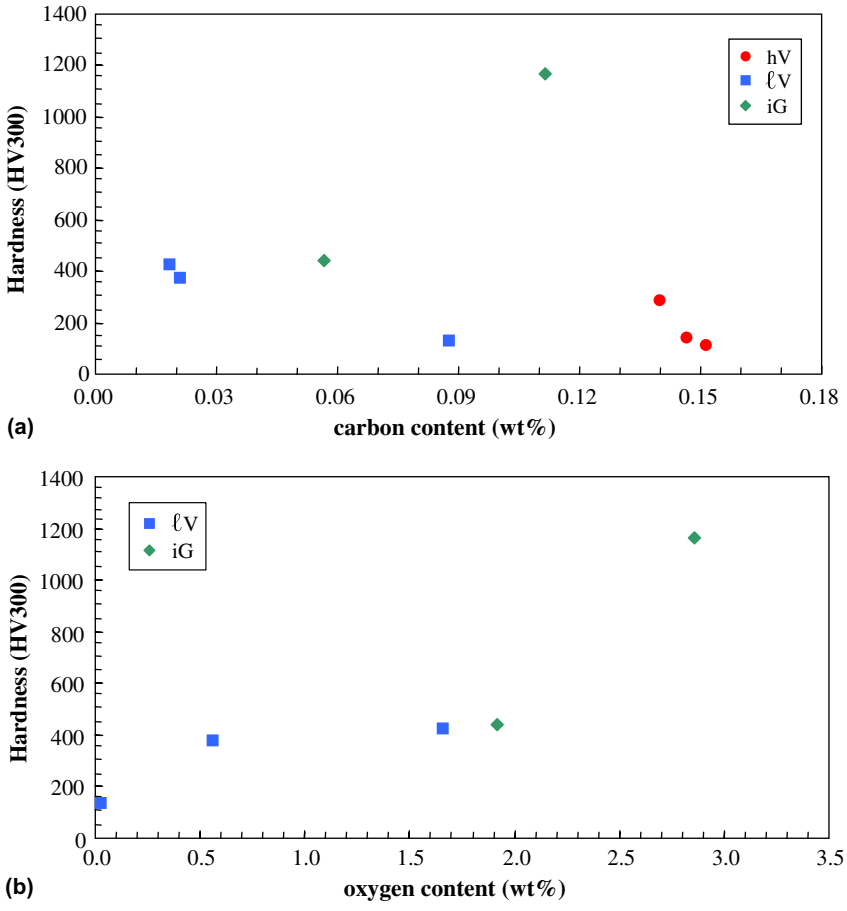

Fig. 12. Microhardness of sintered samples vs. the impurity (carbon and oxygen) contents.

5. Conclusions

For the first time, a master *decomposition* curve for niobium feedstock was developed and evaluated. This is an important information for powder injection molding of niobium, which can help in optimizing binder composition without additional experiments and can predict the remaining amount of binder during the debinding process. A master *sintering* curve based on the work of sintering has been used to model densification during sintering of niobium. Sintering at 2000 °C for 0.5 h in ℓV atmosphere gave the highest density (98%) with the lowest carbon content

(200 ppm). The oxygen is reduced from 19,000 to 300 ppm after sintering at 2000 °C for 2 h in ℓV atmosphere.

It can be concluded that pure niobium not only can be successfully injection molded, but also can result in dense components. Combination of high temperature (>2000 °C) and ultra-high vacuum (10^{-4} Pa) can give up to theoretical density in injection molded niobium. Impurity control during processing is essential to achieve good mechanical properties.

Acknowledgements

The authors gratefully acknowledge the Ben Franklin Technology Development Authority for funding this research through the Center for Innovative Sintered Products.

References

[1] Aggarwal G, Park SJ, Smid I. Development of niobium powder injection molding. Part I: Feedstock and injection molding. Int J Refract Metals Hard Mater 2006;24:253–62.
[2] Wojcik CG. Processing, properties, and applications of high temperature niobium alloys. In: MRS symposium, vol. 322. Pittsburgh, PA: Materials Research Society; 1994, p. 519–30.
[3] Balke CW. Pure columbium. 85th General meeting of fansteel metallurgical corporation, Milwaukee, WI, April 14, 1944. New York, NY: Electrochemical Society; 1994. p. 89–95.
[4] Klopp WD, Sims CT, Jaffee RI. Vacuum reactions of niobium during sintering. The symposium on columbium (niobium). Washington, DC: John Wiley & Sons, Inc.; 1958. p. 106–20.
[5] Krehl M, Schulze K, Petzow G. The influence of gas atmospheres on the first stage sintering of high-purity niobium powders. Metall Trans A 1984;15A:1111–6.
[6] Levinskii YV, Zaitsevm AB, Polyakov YM, Patrikeev YB. Interrelationship between properties of powders, the pressing and sintering conditions and structure of porous niobium. III. The porous structure of material of sintered niobium powders. Soviet Powder Metall Metal Cer 1990;322:519–30.
[7] Sandim HRZ, Padilha AF. On sinterability of commercial purity of niobium. Key Engg Mat 2001;189-191:296–301.
[8] Grill R, Gnadenberger A. Niobium as mint metal: production–properties–processing. Int J Refract Metals Hard Mater 2006;24:275–82.
[9] German RM, Bose A. Injection molding of metals and ceramics. Princeton, NJ: Metal Powder Industries Federation; 1997.
[10] Smid I, Aggarwal G. Powder injection molding of niobium. Mater Sci Forum 2005;475-479:711–6.
[11] Dropmann MC, Stover D, Buchkremer HP, German RM. Properties and processing of niobium superalloys by injection molding. Adv Powder Metall 1992:213–23.
[12] Muylder JV, Zoubov N, Pourbiax M. Niobium. New York: Oxford; 1966. p. 246–50.
[13] Kissinger HE. Reaction kinetics in differential thermal analysis. Anal Chem 1957;29:1702–6.
[14] Su H, Johnson DL. A practical approach to sintering. J Am Ceramic Soc 1996;79:3211–7.
[15] German RM. Powder Metall Sci. 2nd ed. Princeton, NJ: Metal Powder Industries Federation; 1994.
[16] Humphreys FJ, Hatherly M. Recrystallization and related annealing phenomena. Oxford: Elsevier Science; 1995.
[17] Massalski TB. Binary alloy phase diagrams. Materials Park, OH: ASM International; 1990.
[18] Fromm E, Jehn H. Reactions of niobium and tantalum with gases at high temperature and low pressures. Vacuum 1969;19(4):191–7.
[19] Fromm E, Jehn H. On the phase diagram of the niobium–oxygen system. J Less Common Metals 1968;15(2):242–3.